

Article

# Cavity-Assisted Spin-Orbit Coupling of Ultracold atoms

Lin Dong<sup>1</sup>, Chuanzhou Zhu<sup>1</sup> and Han Pu<sup>1\*</sup>

<sup>1</sup> Department of Physics and Astronomy, Rice Quantum Institute, Rice University, Houston, Texas, 77251-1892, USA

\* Author to whom correspondence should be addressed; hpu@rice.edu

Version March 30, 2015 submitted to Atoms. Typeset by *LATEX* using class file *mdpi.cls*

**Abstract:** We investigate dynamical and static properties of ultracold atoms confined in an optical cavity, where two photon Raman process induces effective coupling between atom's internal degrees of freedom and center-of-mass motion. In the meantime, atomic dynamics exerts a back action to cavity photons. We adopt both mean field and master equation approach to tackle the problem and found surprising modifications to atomic dispersions and dynamical instabilities, arising from the intrinsic nonlinearity of the system. Correspondence between semi-classical and quantum limits is analyzed as well.

**Keywords:** cavity quantum electrodynamics; cold atoms; spin-orbit coupling

## 1. Introduction

When Jaynes and Cummings first studied the time evolution of a two-level atom in an electromagnetic field in a *fully* quantized way in 1960s [1], experimental realization of this ideal theoretical model was out of reach. It was made possible only with the advent of one-atom masers in late 1980s, by Rempe, Walther and Klein [2], who experimentally studied the interaction of a single atom and a single resonant mode of electromagnetic field in a cavity. Jaynes-Cummings model (or J-C Model) serves to bridge our understanding of the relationship between quantum theory of radiation and semi-classical theory of atom-light interaction, and has become one of the most important models in quantum optics and cavity electrodynamics (CQED). In the experiment of Ref. [2], a beam of atoms was used and the atom-light interaction was studied during the transient time when the atoms pass through the cavity. The intensity of the atomic beam is sufficiently low such that at any given time, no more than one atom is inside

20 the cavity. The field of CQED was further advanced by putting a single trapped cold atom [3], and  
21 more recent a condensate of ultracold atoms [4–6,8], inside an optical cavity. In the J-C model, and  
22 many other related CQED models, the focus is the interaction and mutual influence between the cavity  
23 mode and the atomic internal degrees of freedom. The external degrees of freedom of the atom, i.e., its  
24 center-of-mass (COM) motion, is generally neglected. Unlike “hot” atoms, however, cold atoms’ COM  
25 motion in general can no longer be neglected in this “atom + cavity” system, as the COM momentum  
26 of a cold atom will be significantly affected by photon recoil from emission and absorption of even a  
27 single photon. Therefore in a more complete description of the cavity system, one needs to take into  
28 account the interplay among the cavity photons, and both the internal and external atomic degrees of  
29 freedom. Furthermore, when more than one atom is inside the cavity, one should also account for the  
30 cavity photon mediated long-range interaction between atoms. All of these make the “cold atoms +  
31 cavity” system extremely rich and interesting, and truly represent a new frontier in both CQED and cold  
32 atom research.

33 As the same photon affects both the internal states (via inducing a transition between different states of  
34 the atom) and the external COM motion (via photon recoil) of the atom, it naturally induces a coupling  
35 between the two atomic degrees of freedom. Such spin-orbit coupling (SOC) in cold atoms has been  
36 realized in both bosonic [9,10] and fermionic systems [11,12], and has attracted tremendous attention in  
37 recent years [13]. In practice, to avoid spontaneous emission, SOC is induced between two hyperfine  
38 ground states of an atom via a pair of Raman laser beams. Due to its non-Abelian nature, SOC not only  
39 significantly affects the physics of a single atom, but, perhaps more importantly, also profoundly changes  
40 the properties of a many-body system. It is an essential ingredient underlying such diverse phenomena  
41 as topological superconductors/insulators, Majorana and Weyl fermions, spin-Hall effects, etc. [14–18].

42 So far, all the experimental realization of photon-induced SOC in cold atoms employs classical laser  
43 fields to generate the Raman transition. Here the parameters of SOC are determined once the laser  
44 parameters (e.g., intensity, frequency, etc.) are fixed. In a recent work [19], we propose to replace one of  
45 the Raman beams by a plane-wave cavity mode supported by a ring cavity. Around the same time, Feder  
46 considered a situation where both Raman beams are provided by a cavity (cite Feder’s PRA). In this  
47 scheme, as the back-action from the atoms affects the cavity photons, the SOC thus induced becomes  
48 nonlinear and dynamical. By employing a simple mean-field approach, we demonstrated [19] that such a  
49 system indeed possesses interesting nonlinear properties even with just one single atom inside the cavity.  
50 For example, the cavity-assisted SOC dramatically modifies the atomic dispersion relation, in particular,  
51 with the emergence of loop structures under certain circumstances.

52 In the present work, we first briefly review our previous proposal [19], and then theoretically explore  
53 the full quantum mechanical treatment beyond the mean-field formalism, and finally investigate the  
54 correspondence between the quantum and the mean-field treatment. The quantum treatment is carried  
55 out by solving the Master equation for the total density operator, from which we can derive various  
56 quantities of interest, i.e., the cavity photon statistics, the degree of entanglement between the atom  
57 and cavity field, etc. These two different approaches provide a deeper understanding of this intriguing  
58 system.

59 The article is organized as the following: After briefly reviewing key ideas of our previous work and  
60 the mean-field approach in Sec. 2, we develop the full quantum mechanical formalism to the physical

61 system of interest in Sec. 3 and discuss about the intimate correspondence between the two in Sec. 4,  
 62 and finally conclude in Sec. 5.

63 **2. Model Setup and Mean-Field Formalism** As shown schematically in Fig. xxx, we consider a single  
 64 atom being confined by a single-mode unidirectional ring cavity, whose cavity mode together with an  
 65 additional coherent laser beam form a pair of Raman beams that induces transition between two hyperfine  
 66 atomic ground states denoted as  $|\uparrow\rangle$  and  $|\downarrow\rangle$ , while transferring recoil momentum  $\pm 2\hbar q_r \hat{z}$  to the atom.  
 67 The ring cavity has a resonant frequency of  $\omega_c$ , decay rate  $\kappa$ , and is pumped by an external laser field  
 68 with frequency  $\omega_p$  and pumping rate  $\epsilon_p$ . The Hamiltonian under the rotating wave approximation can be  
 69 written as [19],

$$\begin{aligned} \mathcal{H}_{\text{eff}} = & \sum_{\sigma=\uparrow,\downarrow} \int dz \left[ \hat{\psi}_\sigma^\dagger(z) \left( \frac{k^2 + 2\alpha_\sigma q_r k}{2m} + \alpha_\sigma \delta \right) \hat{\psi}_\sigma(z) \right] + \frac{\Omega}{2} \int dz \left[ \hat{\psi}_\uparrow^\dagger(z) \hat{\psi}_\downarrow(z) c + h.c. \right] \\ & + i\epsilon_p (\hat{c}^\dagger - \hat{c}) - \delta_c \hat{c}^\dagger \hat{c}, \end{aligned} \quad (1)$$

70 where, for simplicity, we only consider the atomic COM motion along the  $z$ -axis, which is the direction  
 71 of the photon recoil. In Hamiltonian (1),  $k$  is the atomic COM quasi-momentum (we take  $\hbar = 1$ ) along  
 72 the  $z$ -axis,  $\hat{c}$  is the cavity annihilation operator,  $\hat{\psi}_\sigma(z)$  ( $\sigma = \uparrow, \downarrow$ ) is the atomic operator,  $\alpha_{\uparrow,\downarrow} = \pm 1$ ,  $2\delta$   
 73 represents the two-photon Raman detuning,  $\delta_c = \omega_p - \omega_c$  is the cavity-pump detuning, and  $\Omega$  denotes  
 74 the atom-cavity coupling strength. Finally we will treat the cavity decay phenomenologically, which  
 75 amounts to adding a non-Hermitian term  $-i\kappa \hat{c}^\dagger \hat{c}$  in the above effective Hamiltonian. Note that for a  
 76 quasi-momentum  $k$ , the real momentum for an atom is spin-dependent: it is  $k + q_r$  for  $|\uparrow\rangle$  state and  
 77  $k - q_r$  for  $|\downarrow\rangle$  state.

From Hamiltonian (1), one can easily obtain the Heisenberg equations of motion for both atomic and cavity fields. To proceed, we adopt the mean-field approximation by replacing the operators by their respective expectation values:  $\hat{c} \rightarrow c \equiv \langle \hat{c} \rangle$ ,  $\hat{\psi}_\sigma(z) \rightarrow \psi_\sigma(z) \equiv \langle \hat{\psi}_\sigma(z) \rangle$ . Assuming spatial homogeneity, we further take the plane-wave wave-function for the atomic modes  $\psi_\sigma(z) = e^{ikz} \varphi_\sigma$  with the normalization condition  $|\varphi_\uparrow|^2 + |\varphi_\downarrow|^2 = N_{\text{atom}}$ , where  $N_{\text{atom}}$  is the total number of atoms which we take to be 1 in the current work. The steady-state solution for the photon field is obtained by taking the time derivative of the photon field to be zero, from which we obtain:

$$c = \frac{\epsilon_p - i\frac{\Omega}{2} \varphi_\downarrow^* \varphi_\uparrow}{\kappa - i\delta_c}. \quad (2)$$

78 Inserting this into the equations for atomic fields, we obtain the coupled nonlinear time-dependent  
 79 equations for the two spin components as,

$$i\dot{\varphi}_\uparrow = \left( \frac{k^2}{2m} + q_r k + \delta \right) \varphi_\uparrow + \Omega_{\text{eff}} \varphi_\downarrow, \quad (3)$$

$$i\dot{\varphi}_\downarrow = \left( \frac{k^2}{2m} - q_r k - \delta \right) \varphi_\downarrow + \Omega_{\text{eff}}^* \varphi_\uparrow. \quad (4)$$

80 where  $\Omega_{\text{eff}} \equiv \frac{\Omega}{2} c = \frac{\Omega}{2} \frac{\epsilon_p - i\frac{\Omega}{2} \varphi_\downarrow^* \varphi_\uparrow}{\kappa - i\delta_c}$  is the effective Raman coupling strength between two atomic states.  
 81 The fact that  $\Omega_{\text{eff}}$  depends on the atomic field itself is a manifestation of the nonlinearity arising from the  
 82 atomic back-action to the cavity field.

For a given atomic quasi-momentum  $k$ , we define eigenstate and eigenenergy as the solution of the time-independent version of Eqs. (3) and (4), by replacing  $i(\partial/\partial t)$  with  $\epsilon(k)$ . After some lengthy but straightforward algebra, we find that  $\epsilon(k)$  obeys a quartic equation in the form of

$$4\epsilon^4 + B\epsilon^3 + C\epsilon^2 + D\epsilon + E = 0. \quad (5)$$

- 83 The derivation of the above equation and the explicit expressions of the  $k$ -dependent coefficients  $B$ ,  $C$ ,  
 84  $D$  and  $E$  can be found in our previous work [19].

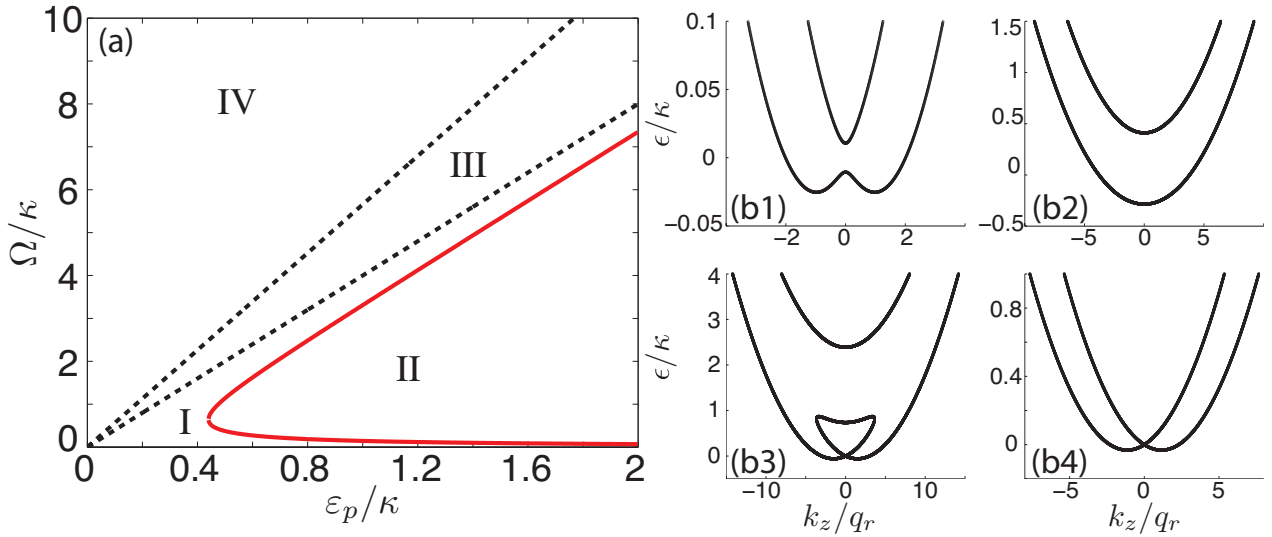


**Figure 1.** (Color Online) Single particle eigen-energy spectrum “phase diagram”. For given parameter  $\delta_c = \kappa$  and  $\delta = 0$ , the dispersion behavior is categorized into four regions, represented from I to IV in (a). From (b1) to (b4), we fix  $\varepsilon_p = \kappa$ . In region I, the dispersion has double minima as shown in (b1) with  $\Omega = 0.03\kappa$ ; region II is enclosed by the red solid curve in (a) and we show the typical point in (b2) ( $\Omega = \kappa$ ) where only single minimum exists in the lower helicity band; region III is enclosed by the black dashed lines in (a) and it is a region where loop structure emerge, as in (b3) with  $\Omega = 5\kappa$ ; finally, in region IV we recover the double minimum dispersion although it’s different from region I by closing the gap at  $k_z = 0$ , as in (b4) with  $\Omega = 8\kappa$ .

We can gain some insights about the general structure of the dispersion relation  $\epsilon(\mathbf{k})$ , e.g. the degeneracy condition and the appearance and disappearance of the loop. In the case of vanishing two-photon detuning (i.e.,  $\delta = 0$ ), simple analysis shows that there should be a total of four regimes, as shown in Fig. 1(a). In region I, the two dispersion branches are gapped, and the lower branch has a double degenerate minima, as shown in Fig. 1(b1). This dispersion curve structure is very similar to the case when both Raman beams are provided by classical coherent laser fields (we shall refer to this as the “classical case”) and the Raman coupling strength is small. In region II, as shown in Fig. 1(b2), the two dispersion branches are still gapped, but the lower branch has a single minimum. This is similar to the classical case with a large Raman coupling strength. Regions III and IV do not have analogs in the classical case. Region III features a loop structure, as shown in Fig. 1(b3), whereas in Region IV, the loop dissolves but the two dispersion branches becomes gapless at  $k = 0$ , as shown in Fig. 1(b4). In the

looped region, the quartic equation (5) yields four real roots. It can be shown [19] that this requires the coupling strength  $\Omega$  to satisfy

$$\Omega_c^{(1)} \equiv 4\epsilon_p \leq \Omega \leq 4\epsilon_p \sqrt{1 + (\delta_c/\kappa)^2} \equiv \Omega_c^{(2)}.$$

- 85 The two dashed lines in Fig. 1(a) represent the two critical values  $\Omega_c^{(1)}$  and  $\Omega_c^{(2)}$ , respectively.

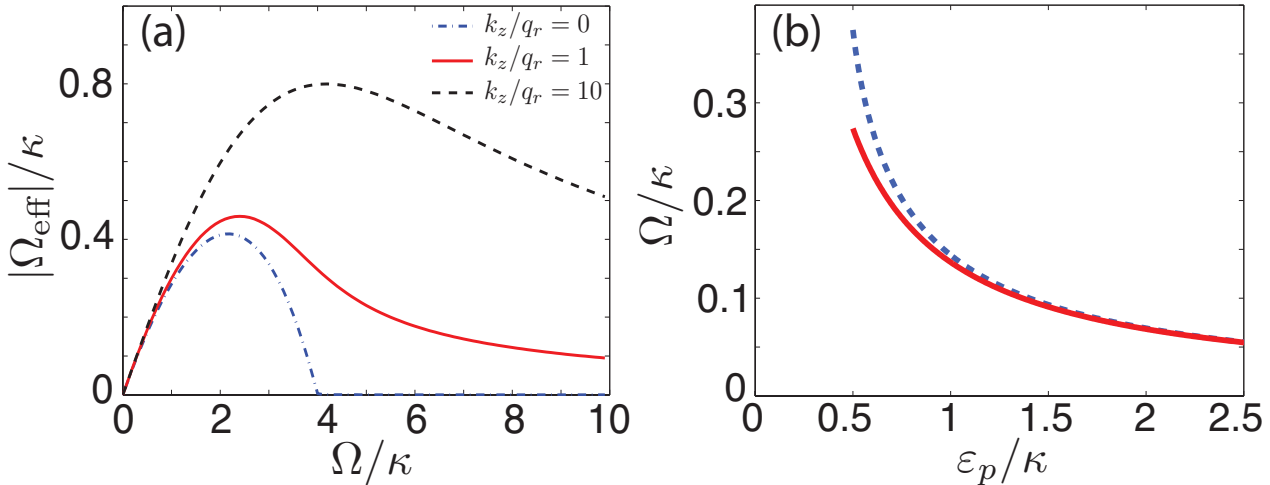


**Figure 2.** (a) Effective Raman coupling  $|\Omega_{\text{eff}}|$  is plotted as a function of atom-photon coupling strength  $\Omega$  for different  $k_z$  values,  $0, q_r, 10q_r$  for blue dash-dot, red solid and black dashed lines. We observe that  $|\Omega_{\text{eff}}|$  does not monotonically increases with  $\Omega$  but rather peaks at an intermediate value, then approaches zero in the large  $\Omega$  limit. Figure (b) shows a comparison between critical boundary of region I and II (red solid curve) and the analytical result (blue dashed line) given in Eq. (6). At large  $\epsilon_p$  limit, the two results match asymptotically well.

- 86 It is instructive examine how the effective Raman coupling strength  $\Omega_{\text{eff}}$  behaves as a function of  $\Omega$ .  
 87 In Fig. 2(a), we plot  $|\Omega_{\text{eff}}|$  for the lowest dispersion branch as a function of  $\Omega$  for different  $k$  values. Note  
 88 that  $|\Omega_{\text{eff}}|^2 = \Omega^2 n_{\text{photon}}/4$  where  $n_{\text{photon}} = |c|^2$  is the steady-state cavity photon number. A few remarks  
 89 can be made based on this plot. First, that  $\Omega_{\text{eff}}$  is different for different  $k$  clearly shows the influence of  
 90 the atomic COM motion on both the atomic internal dynamics and the cavity photon number. Second,  
 91  $|\Omega_{\text{eff}}|$  is not a monotonous function of  $\Omega$ . For given  $k$ ,  $|\Omega_{\text{eff}}|$  increases with  $\Omega$  linearly for small  $\Omega$ . This  
 92 can be intuitively understood as follows. At such weak atom-photon coupling, the back-action from  
 93 the atom to the cavity photon is negligible. The number of cavity photons  $n_{\text{photon}}$  is roughly given by  
 94  $n_{\text{photon}} \approx n_0 = \left| \frac{\epsilon_p}{\kappa - i\delta_c} \right|^2 = \frac{|\epsilon_p|^2}{\kappa^2 + \delta_c^2}$ , where  $n_0$  is the number of cavity photons when the atom is absent. As  
 95 a result, we have  $|\Omega_{\text{eff}}| \approx \Omega \sqrt{n_0}/2$  which is independent of the atomic quasi-momentum  $k$ . On the other  
 96 limit, when  $\Omega$  is very large, the strong atom-cavity coupling strength significantly detunes the cavity  
 97 away from resonance and the cavity photon number  $n_{\text{photon}}$ , and hence  $|\Omega_{\text{eff}}|$ , decreases as a function  
 98 of  $\Omega$ . Such a non-monotonous behavior of  $\Omega_{\text{eff}}$  is a unique feature of the cavity system and a direct  
 99 manifestation of the nonlinearity of the system arising from the back-action of the atom on the cavity  
 100 photon.

From the above analysis, it should also become clear that when the effect of the back-action is weak (which occurs when  $\Omega$  is small and/or  $\epsilon_p$  is large), we should recover the properties of the classical case.

In particular, in the classical case, the lower dispersion branch change from two degenerate minima to a single minimum when the Raman coupling strength exceeds a critical value. Using our notation, this occurs when  $|\Omega_{\text{eff}}|$  exceeds the critical value  $2E_r$  where  $E_r = q_r^2/(2m)$  is the recoil energy. For weak atom-cavity coupling,  $|\Omega_{\text{eff}}| = \frac{\Omega}{2}\sqrt{n_0} = \frac{\Omega}{2}\sqrt{\frac{|\varepsilon_p|^2}{\kappa^2 + \delta_c^2}}$ . Hence the critical value of  $\Omega$  is given by

$$\Omega = 4E_r \frac{\sqrt{\kappa^2 + \delta_c^2}}{\varepsilon_p}. \quad (6)$$

101 In Fig. 2(b), we plot this critical value (blue dashed line) as a function of cavity pump rate  $\varepsilon_p$  and compare  
 102 it with the numerically determined lower boundary (red solid line) between region I and II of Fig. 1(a).  
 103 The two curves overlap with each other when  $\varepsilon_p$  increases. Therefore, as we have expected, in the limit  
 104 of weak atom-cavity coupling and strong cavity pumping, we fully recover the classical case where the  
 105 SOC is induced by two classical laser beams.

106 **3. Master Equation Approach: Full Quantum Mechanical Treatment**

The above discuss is based on the mean-field approach where the cavity field is replaced by a  $c$ -number that represents the photon amplitude. This mean-field treatment relies on two implicit assumptions: (1) the atom-photon correlation is negligible, and (2) the photon field can be well approximated by a coherent state. In order to examine the validity of these assumption, and hence the validity of the mean-field approximation, we now turn to a full quantum treatment based on the Master equation:

$$\dot{\rho} = \frac{1}{i\hbar}[H_{\text{eff}}, \rho] + \mathcal{L}\rho. \quad (7)$$

Here  $\rho$  is the total density operator of the coupled atom-cavity system, the effective Hamiltonian  $H_{\text{eff}}$  is the same as in Eq. (1). The dissipation arising from cavity decay is modelled by the Liouvillean term in the standard form of Lindblad superoperator [20,21],

$$\mathcal{L}\rho = \kappa(2c\rho c^\dagger - c^\dagger c\rho - \rho c^\dagger c). \quad (8)$$

107 Again, due to spatial homogeneity, we decouple momentum eigenstates by taking the plane-wave ansatz  
 108 for the atomic modes as  $\hat{\psi}_\sigma(z) = e^{ikz}\hat{\psi}_\sigma$ . As there is no coupling between atomic operators with different  
 109  $k$ , we can work in the subspace for a fixed value of  $k$ . Here we explicitly write the commutator in Eq. (7),  
 110 for a given atomic quasi-momenutm  $k$ , as,

$$\begin{aligned} [\mathcal{H}_{\text{eff}}(k), \rho] &= \left(\frac{k^2}{2m} + \frac{q_r k}{m} + \delta\right) \left(\hat{\psi}_\uparrow^\dagger \hat{\psi}_\uparrow \rho - \rho \hat{\psi}_\uparrow^\dagger \hat{\psi}_\uparrow\right) + \left(\frac{k^2}{2m} - \frac{q_r k}{m} - \delta\right) \left(\hat{\psi}_\downarrow^\dagger \hat{\psi}_\downarrow \rho - \rho \hat{\psi}_\downarrow^\dagger \hat{\psi}_\downarrow\right) \\ &\quad + \frac{\Omega}{2} \left(\hat{\psi}_\uparrow^\dagger \hat{\psi}_\downarrow \hat{c}\rho + \hat{c}^\dagger \hat{\psi}_\downarrow^\dagger \hat{\psi}_\uparrow \rho - \rho \hat{\psi}_\uparrow^\dagger \hat{\psi}_\downarrow c - \rho \hat{c}^\dagger \hat{\psi}_\downarrow^\dagger \hat{\psi}_\uparrow\right) \\ &\quad + i\varepsilon_p (\hat{c}^\dagger \rho - \hat{c}\rho - \rho \hat{c}^\dagger + \rho \hat{c}) - \delta_c (\hat{c}^\dagger \hat{c}\rho - \rho \hat{c}^\dagger \hat{c}). \end{aligned} \quad (9)$$

111 Note that if the photon recoil  $q_r = 0$ , which occurs when the cavity mode and the external laser beams  
 112 are co-propagating, the COM kinetic energy terms  $k^2/(2m)$  can be gauged away after a simple gauge  
 113 transformation. Our model is then reduced to the J-C model and the atomic COM motion does not play  
 114 a role. To solve the Master equation (7), we choose our basis states as direct product states of photon

115 Fock state  $|n\rangle$  and atomic internal state  $|\sigma\rangle$ :  $|n; \sigma\rangle \equiv |n\rangle \otimes |\sigma\rangle$ , where non-negative integer  $n$  denotes  
 116 cavity photon number. Our goal is to calculate the entire matrix elements of the density operator under  
 117 this set of basis states, denoted by  $\langle m; \sigma | \rho | n; \sigma' \rangle \equiv \rho_{mn}^{\sigma\sigma'}$ . We found the governing equation for the matrix  
 118 element can be written as,

$$\begin{aligned} \frac{d}{dt} \rho_{mn}^{\sigma\sigma'} &= -i \left( \frac{k^2}{2m} + \frac{q_r k}{m} + \delta \right) (\delta_{\sigma\uparrow} - \delta_{\sigma'\uparrow}) \rho_{mn}^{\sigma\sigma'} - i \left( \frac{\mathbf{k}^2}{2m} - \frac{q_r k_z}{m} - \delta \right) (\delta_{\sigma\downarrow} - \delta_{\sigma'\downarrow}) \rho_{mn}^{\sigma\sigma'} \\ &+ \frac{\Omega}{2i} (\delta_{\sigma\uparrow} \sqrt{m+1} \rho_{m+1n}^{\bar{\sigma}\sigma'} + \delta_{\sigma\downarrow} \sqrt{m} \rho_{m-1n}^{\bar{\sigma}\sigma'} - \delta_{\sigma'\uparrow} \sqrt{n+1} \rho_{mn+1}^{\sigma\bar{\sigma}'} - \delta_{\sigma'\downarrow} \sqrt{n} \rho_{mn-1}^{\sigma\bar{\sigma}'}) \\ &+ \varepsilon_p \left( \sqrt{m} \rho_{m-1n}^{\sigma\sigma'} - \sqrt{m+1} \rho_{m+1n}^{\sigma\sigma'} + \sqrt{n} \rho_{mn-1}^{\sigma\sigma'} - \sqrt{n+1} \rho_{mn+1}^{\sigma\sigma'} \right) \\ &+ i \delta_c (m-n) \rho_{mn}^{\sigma\sigma'} + \kappa \left( 2\sqrt{m+1} \sqrt{n+1} \rho_{m+1n+1}^{\sigma\sigma'} - (m+n) \rho_{mn}^{\sigma\sigma'} \right), \end{aligned} \quad (10)$$

119 where  $\bar{\sigma}$  represents the flip-spin value, i.e.  $\bar{\uparrow} = \downarrow$  and  $\bar{\downarrow} = \uparrow$ .

120 With Eq. (10), we can study the dynamical evolution of the density operator  $\rho$  for a given initial state.  
 121 Obviously, we need to introduce a sufficiently large photon number cutoff. Once we obtain the density  
 122 operator, all relevant physical quantities can be readily calculated. An example is given in Fig. 3, where  
 123 we show the time evolution of the cavity photon number  $n = \text{Tr}[\rho \hat{n}] = \text{Tr}[\rho \hat{c}^\dagger \hat{c}]$  for the initial state  $|0; \uparrow\rangle$ .  
 124 The three different curves in Fig. 3 correspond to different atomic quasi-momentum  $k$ .

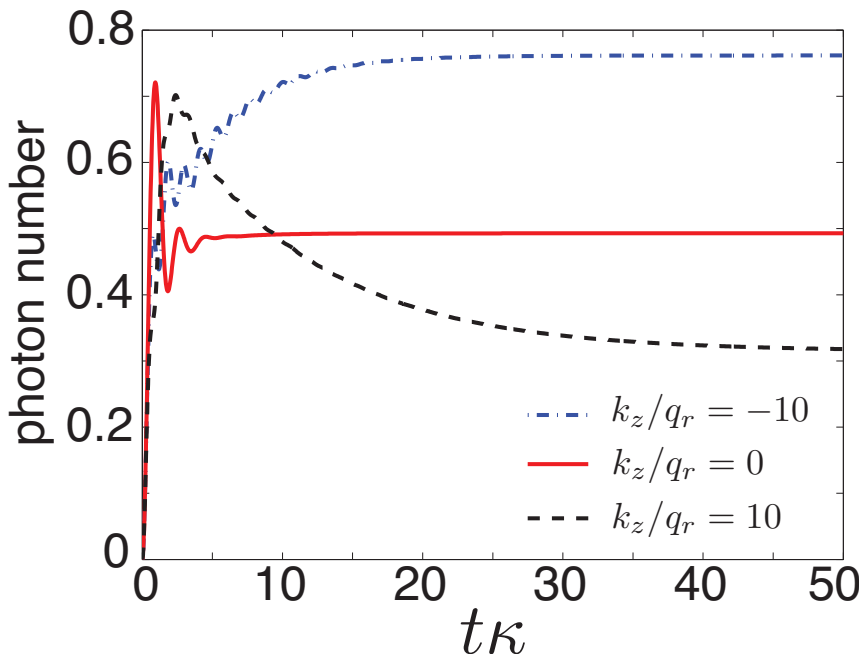


**Figure 3.** Time evolution of cavity photon number. The initial state is given by  $\rho_0 = |0; \uparrow\rangle$  and we consider the same parameter as in Fig. 4(a) with  $k/q_r = -10, 0, 10$ . The steady states correspond to red dashed line results at corresponding  $k_z$  values in Fig. 4(a), which is obtained by equating the RHS of Eq. 10 to zero.

125 As evidenced in Fig. 3, due to the presence of cavity decay, a steady state will eventually be reached.  
 126 Let us now focus on the properties of this steady state. The steady-state density operator matrix elements  
 127 can be obtained by equating the RHS of Eq. (10) to zero. The red dashed lines in Fig. 4(a)-(c) represent  
 128 the steady-state photon number as functions of atomic quasi-momentum  $k$ . The horizontal arrows in the

129 plot represent the cavity photon number by setting  $q_r = 0$ , in which case our model reduces to the J-C  
 130 model and all physical quantities become  $k$ -independent.

To have a better understanding of the photon statistics, we study the steady-state photon number fluctuation. Specifically, we calculate the normalized photon fluctuation defined as

$$\Delta_n = \frac{\langle (\Delta n)^2 \rangle}{\langle \hat{n} \rangle} = \frac{\langle \hat{n}^2 \rangle - \langle \hat{n} \rangle^2}{\langle \hat{n} \rangle},$$

131 where the expectation values of the operators are obtained with the help of the steady-state density  
 132 operator. For a coherent cavity field, the photon fluctuation is Poissonian and we have  $\Delta_n = 1$ . The  
 133 solid curves in Fig. 4(d)-(f) represent  $\Delta_n$  (left vertical axis) as functions of  $k$ , and the horizontal arrows  
 134 pointing to left give the values of  $\Delta_n$  from the J-C model by setting  $q_r = 0$ . We note that the J-C model  
 135 always predicts a super-Poissonian photon statistics, whereas our model gives super-Poissonian photon  
 136 statistics only for small atomic quasi-momentum, but Poissonian statistics as  $k/q_r \rightarrow \pm\infty$ .

137 Finally to characterize the correlation between the atom and the cavity field, we investigate the  
 138 so-called negativity [22] which measures the atom-cavity entanglement. The negativity is defined as  
 139  $\mathcal{N}(\rho) = (\frac{\|\rho^{TA}\|_1 - 1}{2})$ , where  $\rho^{TA}$  is the partial transpose of the density operator with respect to either  
 140 the atom subsystem or the cavity subsystem, and  $\|\rho^{TA}\|_1$  denotes its trace norm with the definition  
 141  $\|\hat{A}\|_1 \equiv \text{Tr}[\sqrt{\hat{A}^\dagger \hat{A}}]$ . A negativity of zero indicates that the two subsystems (the atom and the cavity,  
 142 in our case) are unentangled, whereas a positive negativity means that finite degree of entanglement is  
 143 present. The dashed curves in Fig. 4(d)-(f) represent the negativity (right vertical axis) in the steady state  
 144 as functions of  $k$ , and the horizontal arrows pointing to right give the values of the negativity from the  
 145 J-C model by setting  $q_r = 0$ . One can observe that for the chosen parameters, the J-C model always  
 146 predicts a finite degree of entanglement between the atom and the cavity field. By contrast, the degree  
 147 of entanglement in our model weakens when  $k/q_r \rightarrow \pm\infty$ .

#### 148 4. Discussions

149 In the previous two sections, we have presented two different methods for studying the system. We  
 150 are now in a position to discuss their connections.

151 In Fig. 4(a)-(c), in addition to the steady-state photon number obtained from the quantum treatment  
 152 (dashed curves), we also plot the photon number  $n_{\text{photon}} = |c|^2$  obtained from the mean-field approach  
 153 (solid curves), with  $c$  given in Eq. (2). In the quantum treatment, the steady-state density matrix is  
 154 obtained by solving a set of linear equations. For a given  $k$ , the solution is unique. Hence we only  
 155 get one steady-state photon number for a given atomic quasi-momentum. On the other hand, the  
 156 mean-field treatment allows multiple steady-state solutions corresponding to different real roots of the  
 157 quartic equation (5). Hence a single  $k$  value is associated with more than one steady-state photon number.  
 158 However, due to the nonlinearity intrinsic in the mean-field method, not all steady-states are dynamically  
 159 stable. A straightforward stability analysis allows us to quantify the dynamical stability of the mean-field  
 160 states, as we did in Ref. [19]. The information of the stability of the mean-field states are encoded in  
 161 the color of the solid curves. Those stable states are represented by black color, while any other color  
 162 indicates an unstable state, and the color represents the decay rate (see the color bar) of the corresponding  
 163 state. From Fig. 4(a)-(c), we clearly see that at large atomic quasi-momentum  $k/q_r \rightarrow \pm\infty$ , the Master

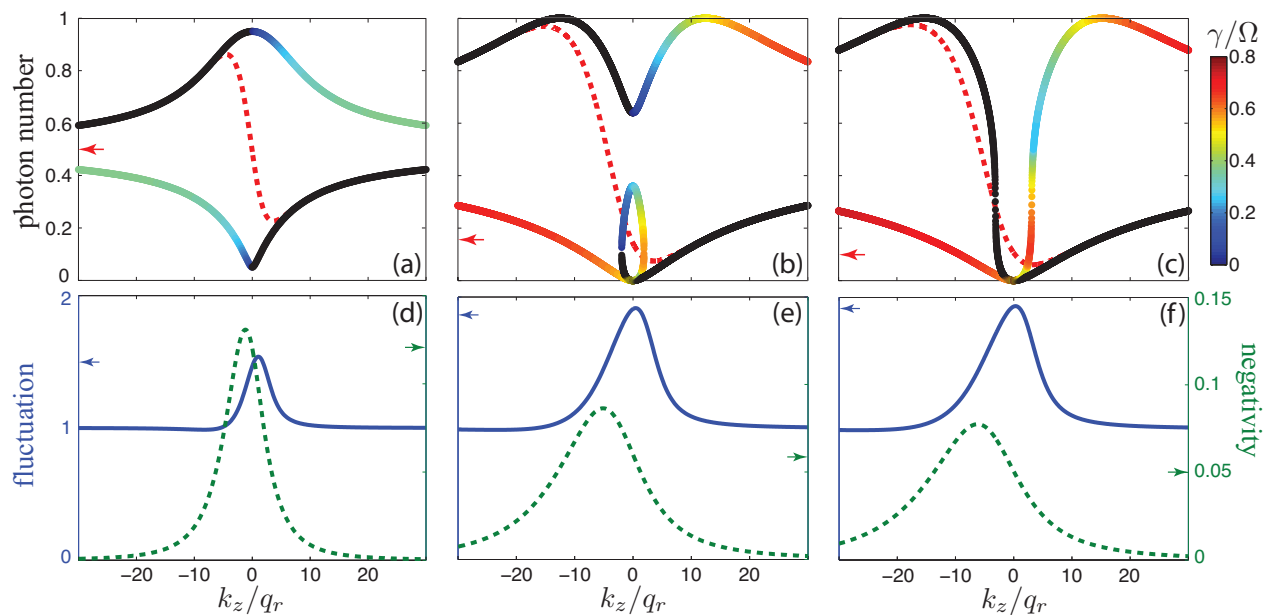


**Figure 4.** (Color Online) Photon number comparison between semi-classical mean field result and full quantum mechanical master equation solution. From (a) to (c),  $\Omega = 3\kappa, 5.6\kappa, 6\kappa$  and colorbar represents the renormalized decay rate  $\gamma/\Omega$  of unstable states and red dashed lines are master equation solutions. Figures from (d) to (f) show the corresponding photon number fluctuation (blue solid curve) and negativity (green dashed line). Other parameters are  $\varepsilon_p = \kappa, \delta_c = \kappa, \delta = 0$  and  $\kappa = 1$  in the dimensionless unit. Although we have chosen  $q_r = 0.22$  in our units (based on a realistic experimental parameter estimate) throughout all figures, we use arrows on vertical axis to denote results concerning  $q_r = 0$  limit.

equation result overlaps with the stable mean-field branch; while at small  $|k|$ , the quantum result deviates significantly away from the mean-field result.

The agreement for large  $|k|$  and the discrepancy at small  $|k|$  are both consistent with the results of the negativity and photon number fluctuations as presented in Fig. 4(d)-(f): At large  $|k|$ , the negativity is small (i.e., atom-cavity entanglement is weak) and the photon number fluctuation tends to Poissonian (i.e., the photon field is well approximated by a coherent state), this is exactly the regime where we expect the mean-field approximation is valid. By contrast, for small  $|k|$ , the quantum calculation indicates that there is non-negligible entanglement between the atom and the cavity field, and the cavity field itself cannot be assumed as a coherent state. Hence the mean-field assumption is no longer valid.

There is actually a rather simple explanation why the mean-field approximation only works for large  $|k|$ . Consider a Raman transition process where the atom jumps from  $|\uparrow\rangle$  to  $|\downarrow\rangle$ . The quasi-momentum  $k$  does not change during this process, however the real momentum changes from  $k + q_r$  to  $k - q_r$ . Therefore the effective two-photon Raman detuning is not just  $2\delta$ , but  $2\delta + 2q_r k/m$ , where the extra term comes from the change of the COM kinetic energy of the atom. In the examples we presented in this work, we have take  $\delta = 0$ . Hence the Raman transition is only near-resonant for small  $|k|$ , and becomes off-resonant for large  $|k|$ . In other words, as  $|k|$  increases, the effective atom-cavity coupling and the atomic back-action to cavity are both weakened. This explains why the mean-field assumption becomes valid in this regime.

## 5. Conclusion and Outlook

In this work, we have studied spin-orbit coupled cold atoms inside a ring cavity system, employing both the mean-field theory and the full quantum mechanical Master equation approach. By treating both light and atom on equal footing and seeking the self-consistent solution in both approaches, we have found cavity-assisted SOC dramatically modified atomic dispersion relation, intriguing dynamical instabilities, and atom's back-action onto cavity field also leads to non-trivial atom-photon coupling that are fundamentally different from either the system with classical-laser induced SOC in the absence of the cavity or the J-C model where the atomic COM motion is neglected (i.e., by taking  $q_r = 0$ ). We have also explored correspondence and discussed the relationship between the mean-field and the quantum approaches. The two distinctively different approaches provide us with a deeper understanding and complementary insights into this system. We conclude that the synthesis of cavity QED and SOC is not a trivial combination and interesting new physics will emerge in this setting.

## Acknowledgments

This work is supported by the NSF and the Welch Foundation (Grant No. C-1669);

## Author Contributions

H.P. conceived the idea of the project, L.D. and C. Z. explored the theoretical and numerical aspects of the physics. All authors contributed to writing and revising the manuscript and participated in the discussions about this work.

200 **Conflicts of Interest**

201 The authors declare no conflict of interest.

202 **References**

- 203 1. Jaynes, E.; Cummings, F. Comparison of quantum and semiclassical radiation theories with  
204 application to the beam maser. *Proc. IEEE* **1963**, *51*(1), 89-109
- 205 2. Rempe, G.; Walther, H.; Klein, N. Observation of quantum collapse and revival in a one-atom  
206 maser. *Phys. Rev. Lett.* **1987**, *58* (4), 353-356
- 207 3. Ye, J.; Vernooy, D. W., Kimble, H. J. Trapping of single atoms in cavity QED. *Phys. Rev. Lett.*  
208 **1999** *83*, 4987
- 209 4. Brennecke, F.; Donner, T.; Ritter, S.; Bourdel, T.; Kohl, M.; Esslinger, T. Cavity QED with a  
210 Bose-Einstein condensate. *Nature* **2007**, *450*, 268
- 211 5. Colombe, Y.; Steinmetz, T.; Dubois, G.; Linke, F.; Hunger, D.; Reichel, J. Strong atom-field  
212 coupling for Bose-Einstein condensates in an optical cavity on a chip. *Nature* **2007**, *450*, 272
- 213 6. Slama, S.; Bux, S.; Krenz, G.; Zimmermann, C.; Courteille, PH. W. Superradiant Rayleigh  
214 Scattering and Collective Atomic Recoil Lasing in a Ring Cavity. *Phys. Rev. Lett.* **2007**, *98*,  
215 053603
- 216 7. Dicke, R. H. Coherence in spontaneous radiation processes. *Phys. Rev.* **1954**, *93*, 99-110
- 217 8. Baumann. K.; Guerlin, C.; Brennecke, F.; Esslinger, T. Dicke quantum phase transition with a  
218 superfluid gas in an optical cavity. *Nature* **2010**, *464*, 1301-1306
- 219 9. Lin, Y. -J.; Jimenez-Garcia, K.; Spielman, I. B. A spin-orbit coupled Bose-Einstein condensate.  
220 *Nature* **2011**, *471*, 83
- 221 10. Lin, Y.-J.; Compton, R. L.; Jimenez-Garcia, K.; Phillips, W. D.; Porto, J. V.; Spielman, I. B. A  
222 synthetic electric force acting on neutral atoms. *Nat. Phys.* **2011**, *7*, 531
- 223 11. Wang, P.; Yu, Z.-Q.; Fu, Z.; Miao, J.; Huang, L.; Chai, S.; Zhai, H.; Zhang, J. Spin-Orbit Coupled  
224 Degenerate Fermi Gases. *Phys. Rev. Lett.* **2012**, *109*, 095301
- 225 12. Cheuk, L. W.; Sommer, A. T.; Hadzibabic, Z.; Yefsah, T.; Bakr, W. S.; Zwierlein, M. W.  
226 Spin-Injection Spectroscopy of a Spin-Orbit Coupled Fermi Gas. *Phys. Rev. Lett.* **2012**, *109*,  
227 095302
- 228 13. Galitski, V; Spielman, I. B. Spin-orbit coupling in quantum gases. *Nature* **2013**, *494* 7435
- 229 14. Hasan, M. Z.; Kane, C. L. Colloquium: Topological insulators. *Rev. Mod. Phys.* **2010**, *82*,  
230 3045-3067
- 231 15. Sau, J. D.; Lutchyn, R. M.; Tewari, S.; Sarma Das, S. Generic New Platform for Topological  
232 Quantum Computation Using Semiconductor Heterostructures. *Phys. Rev. Lett.* **2010**, *104*, 040502
- 233 16. Burkov, A. A.; Balents, L. Weyl Semimetal in a Topological Insulator Multilayer. *Phys. Rev. Lett.*  
234 **2011**, *107*,127205
- 235 17. Sinova, J.; Cilcer, D.; Niu, Q.; Sinitzyn, N.; Jungwirth, T.; MacDonald, A. Universal Intrinsic Spin  
236 Hall Effect. *Phys. Rev. Lett.* **2004**, *92*, 126603
- 237 18. Kato, Y. K.; Myers, R. C.; Gossard, A. C.; Awschalom, D. D. Observation of the spin Hall effect  
238 in semiconductors. *Science* **2004**, *306*, 1910-1913

- 239 19. Dong, L.; Zhou, L.; Wu, B.; Ramachandhran, B.; Pu H. Cavity-assisted dynamical spin-orbit  
240 coupling in cold atoms. *Phys. Rev. A* **2014**, *89*, 011602(R)
- 241 20. Kossakowski, A. On quantum statistical mechanics of non-Hamiltonian systems. *Rep. Math. Phys.*  
242 **1972**, *3* (4), 247
- 243 21. Lindblad, G. On the generators of quantum dynamical semigroups. *Commun. Math. Phys.* **1976**,  
244 *48* (2): 119
- 245 22. Vidal, G.; Werner, R. F.; Computable measure of entanglement. *Phys. Rev. A* **2002**, *65*, 032314

246 © March 30, 2015 by the authors; submitted to *Atoms* for possible open access  
247 publication under the terms and conditions of the Creative Commons Attribution license  
248 <http://creativecommons.org/licenses/by/4.0/>.